Journal of Optics

PAPER • OPEN ACCESS

Optical non-volatile correction of SERS wavelength using optical pumping

To cite this article: Mohammad Ali Shameli *et al* 2023 *J. Opt.* **25** 085001

View the article online for updates and enhancements.

You may also like

- Fabrication of antireflective silver-capped tin oxide nano-obelisk arrays as high sensitive SERS substrate
Abdul Rasheed Paloly and M Junaid Bushiri
- Red shifted spectral dependence of the SERS enhancement in a random array of gold nanoparticles covered with a silica shell: extinction versus scattering
C D'Andrea, A Irrera, B Fazio et al.
- Ag films annealed in a nanoscale limited area for surface-enhanced Raman scattering detection
Dan Jiang, Shuping Xu, Hailong Wang et al.

This content was downloaded from IP address 212.71.9.150 on 09/08/2023 at 10:50

OPEN ACCESS
IOP Publishing
Journal of Optics
J. Opt. **25** (2023) 085001 (11pp)
https://doi.org/10.1088/2040-8986/ace0cc

Optical non-volatile correction of SERS wavelength using optical pumping

Mohammad Ali Shameli[1,*], **Mohammad Reza Eskandari**[2] **and Reza Safian**[3]

[1] Department of Information Engineering, University of Padua, 35131 Padova, Italy
[2] Department of Electrical Engineering, Shahreza Campus, University of Isfahan, Isfahan, Iran
[3] imec, USA, 194 NeoCityWay, Kissimmee, FL 34744, United States of America

E-mail: mohammadali.shameli@unipd.it

Received 21 April 2023, revised 9 June 2023
Accepted for publication 22 June 2023
Published 29 June 2023

Abstract

In this paper, we propose a reconfigurable two-dimensional photonic crystal (PC) made from a new ultralow loss phase change material for detecting and imaging applications of surface-enhanced Raman scattering (SERS). The proposed all-dielectric structure is composed of identical holes periodically distributed on Sb_2S_3 as a substrate, tuned by optical pumping. The proposed PC is investigated using full-wave simulation of the CST with the finite-difference frequency domain method over a wide bandwidth of optical wavelengths. In this study, compensation for the error of the Fano resonance wavelength due to the fabrication process is realized through tuning optical pumping applied to the configuration. Also, the numerical results show the designed PC supports two high-quality Fano resonance modes, leading to uniform and high field enhancement with a SERS enhancement factor of 1.23×10^{12}, which is significant for the application of SERS enhancement.

Keywords: SERS, photonic crystal, reconfigurable structure, phase change material, optical pumping, Fano resonace

(Some figures may appear in colour only in the online journal)

1. Introduction

Raman scattering, a kind of inelastic scattering, describes the interaction of incident photons with matter that causes decreasing (stokes Raman scattering) or increasing (anti-stokes Raman scattering) in energy and changing light direction [1–3]. By measuring the energy differences between an incident and scattered electromagnetic wave, data about the vibrational energy and frequencies can be obtained, which are related to the specific molecule, and has several applications in imaging [1], material science [2], biology [3, 4], and medicine [5]. One of the acute side effects of using this phenomenon, especially for molecular detection, is the intrinsically low cross-section level of Raman scattering, which is about (10-24-10-30 cm^2 sr^{-1}), resulting in limited detection at the Mili molar level [6–8]. Compensating for this problem and boosting Raman signals, we use a non-invasive and sensitive technique named surface-enhanced Raman scattering (SERS) that has been rapidly extended by researchers [6–8].

Primary techniques of SERS for a high level of field enhancement were based on plasmonic structures [9–12]. In one method, the intensity of electromagnetic fields could be tuned by designing metallic nanostructures to generate electromagnetic hotspots at the place of molecular [9, 10]. A higher-order metal array, for instance, enables light focusing via surface plasmon-polariton excitation. Tuning parameters of the proposed structure, such as grating periodicity and metal thickness, lead to optimal excitation of SPP and the SERS enhancement by a factor of four [9]. Iqbal *et al* [10]

* Author to whom any correspondence should be addressed.

Original content from this work may be used under the terms of the Creative Commons Attribution 4.0 licence. Any further distribution of this work must maintain attribution to the author(s) and the title of the work, journal citation and DOI.

 © 2023 The Author(s). Published by IOP Publishing Ltd

states that 1D sinusoidal-shape gold grating reaches the SERS enhancement factor of $EF = 6.4 \times 10^9$, which is five times greater than the EF of the rectangular grating ($EF = 1.2 \times 10^9$).

Another effective method for reaching a high level of enhancement for SERS is the utilization of metallic resonators such as Au, Ag, Cu, and also Al to generate localized surface plasmon resonances (LSPR); coupling between the incoming light and this resonance leads to the second resonance that creates a plasmonic hotspot and increases the concentration of electromagnetic waves for both excitation and emission resulting in improvement of SERS intensity [7]. Based on this method in [11], Au nanoparticle array were placed on the memory polyurethane substrate as reconfigurable materials to tune the LSRP, which has significant potential in SERS applications. In [12], gold nanorods were assembled on gratings, which resulted in about a 30-fold increase in SERS signals, due to the coupling between the LSPR of the gold nanoparticles and the guided modes of the gratings. Zhang *et al* [13] proposed nanostructures of hat-shaped MoS_2 hierarchical and Ag nanoparticles with different space curvatures to enhance hot spots for SERS. MoS_2 as a nanosheet and metallic nanoparticles were presented for SERS enhancement [14]. Even though all these efforts have been made to enhance SERS, plasmonic loss and oxidation in metallic structures have limited their performance [9–12]. Also [15], proposed a two-dimensional (2D) semimetal material made of molybdenum carbide that can reduce the problems of plasmonic structures.

Alternative to plasmonic structures, dielectric ones without a probability of oxidation can compensate for ohmic loss and achieve a higher level of SERS enhancement [8, 16–19]. In one work, the excitation of Fabry–Perot resonances is used for the application of SERS [16]. Pirotta *et al* [17] proposed a fully dielectric periodic structure that couples the optical pump to the block modes. In the proposed work, a photoluminescence experiment represented an enhancement of two orders of magnitude, in which the SERS reached about 200. The other dielectric structure that can be used for SERS enhancement is a silicon metasurface with tip shape resonators that induce local electric field resonances, which are much stronger than LSPR. This dielectric metasurface with a quasi-continuous spectrum can be employed as a SERS substrate without ohmic loss [18]. Sabri *et al* [8] proposed an all-dielectric photonic crystal (PC) for enhancement and uniformity of SERS due to the high-quality factor resonance of dielectric PCs. This work realized 97% of uniformity by the interaction of two PCs modes and a maximum field enhancement of 70. In other research, proposing an all-dielectric PC metasurface that supports bound states in the continuum provided narrow resonances with six orders of magnitude of enhancement factor and represented significant potential in SERS applications [19].

Among the previous studies of all-dielectric structures for SERS, PCs capable of enabling high-quality guided-mode Fano resonances stand out as one of the most promising candidates for SERS enhancement. These Fano resonances, realized by providing 1D or 2D periodic index contrast in PCs, have different field distributions, which can improve the electric field intensity in a particular part of the structure. Researchers have developed many works on all-dielectric PCs in recent years. Slotted PC waveguides (SPCWs) are designed for sensing at mid-infrared wavelengths that are engineered to increase effective sensitivity through resonant tapering [20]. In the mid-infrared wavelengths [21], proposed a SPCW structure with a triangular lattice pattern of ring-shaped holes to enhance the sensor's sensitivity. Elliptical-hole planar PC (EPhC), composed of PC made of silicon and a triangular lattice of holes, increases the Q factor and sensitivity of the structure for measuring the refractive index variation used in the coating of the EPhC [22]. Another work proposed by [23] for the switching application is a triangular lattice planar PC made of silicon with nanocavity incorporated in the center of the structure. Despite all of the previous studies proposing all-dielectric substrates to achieve different applications, such as high SERS enhancement, uniformity [20–23] and the possibility of tuning the resonance wavelength were overlooked in the previous work [8, 16–19]. In this paper, to address this critical problem, we developed a new reconfigurable all-dielectric 2D PC that is composed of active materials. In this reconfigurable structure, the two Fano resonances provide tunable, lossless, uniform, and high-level enhancement of electromagnetic field, which is essential for SERS applications.

In recent years, reconfigurable structures have attracted enormous interest due to their tunable functionality without physical changes [24–27]. These structures, controlled by a different stimulus, such as bias voltage or optical pumping, could be used for the development of photonic devices. The tuning of the bias voltage in [24] results in changing the electron accumulation in the ITO layer and controlling the refractive index, thereby controlling the polarization of the reflected wave. In [25], a reflective metasurface platform based on $Ge_2Sb_2Te_5$ (GST) was developed to realize a tunable lens. A reconfigurable nano-antenna is proposed in [26], which uses 4-N,N-dimethylamino-4'-N'-methyl-stilbazolium tosylate (DAST) as an optoelectronic material, tuned by a bias voltage, and can be adapted in real-time to change gain and angle. Moreover, using loss-less optoelectronic materials realized a rotational freedom thin-film solar cell [27]. Another reconfigurable structure was designed by dielectric metasurface via insulator to the metal transition of the VO_2 [28]. A modulator is another device realized by a structure of PC fiber that changes the wavelength of operation between 1414 nm and 1700 nm through tuning bias voltage applied to the liquid crystal LC [29]. In each structure, active materials add reconfigurable features to the devices, however, optoelectronic materials like DAST are not memorable [26, 27], and phase-change materials such as GST, VO_2, and liquid crystal [24, 25, 28, 29] add loss to the structure, which is not appropriate for the application of SERS.

In this paper, we design a reconfigurable PC using Sb_2S_3, a novel ultralow loss phase change material [30], which is tuned by optical pumping and provides a novel perspective on SERS enhancement. This work proposes a PC with uniform high SERS enhancements, and the ability to reconfigure the structure is one of its most impressive features. The importance of this tunability becomes obvious in correcting the error in Raman resonance wavelength, which may occur

during the fabrication process, especially in the fabrication of the PC with the exact location and radius of holes. Failure to achieve this accuracy will result in shifting the calculated resonances, which have not been considered in previous works [8–12, 16–19, 24–30], leading to wasted effort in designing and analyzing structures for SERS enhancement.

The organization of this paper starts by explaining a 2D PC and investigating the structure by full-wave simulation of CST with the finite difference frequency domain (FDFD) method. Then, we study the possibility of controlling the wavelength resonance of the PC, which could be used for sensing different molecules of different sizes. Furthermore, the next investigation involves correcting the error in Raman resonance wavelength, which may be unintentionally realized during fabrication by optical pumping applied to the Sb_2S_3 substrate. Finally, we discuss the uniformity, average, and maximum SERS enhancement of the proposed reconfigurable PC.

2. The proposed structure and the background theory

Fano resonance is a kind of resonance that gives rise to an asymmetry line shape, which occurs due to interference between two scattering amplitudes: the continuum states and discrete states (the resonant states) [31]. To occur such a resonance, the energy of the resonant state should be close to the continuum state; in this situation, the amplitude of continuum states varies slowly, and the resonant ones vary quickly in terms of amplitude and phase. To realize such a structure with Fano resonances, we start with the 2D PC structure of [8] composed of identical holes periodically distributed on the Sb_2S_3 substrate (see figure 1), and works in the wavelength range of 1400–1700 nm [32]. In our structure, the continuum states are the states of Sb_2S_3 film without PC structure, and the discrete states are confined by the holes and Sb_2S_3 film [31, 33]. At large optical wavelengths, reducing light scattering and background interference cause increases sensitivity, spatial resolution, and skin penetration for imaging and spectroscopy detection [32]. Also, in some applications, such as homeland security and chemical detection and measurement, Raman spectroscopy should be applied at infrared wavelengths [4, 13, 34]. For example, this work [34] suggested a wavelength of 1550 nm with an appropriate surface-enhanced Raman-active substrate, which provides equal sensitivity and could be used in the measurement of some chemicals of interest. Safety for the user during the excitation of a 1550 nm laser is another significant feature described in [34], especially in cases of permanent retinal damage. Also [13], and [4] used 1550 nm laser excitation for SERS performance in the applications of picomolar detection and security, respectively.

Figure 1 shows a perspective view of the structure in which t is the thickness of the substrate, R is the radius of the holes, Px and Py are periodic parameters in the x-axis and y-axis directions of the coordinate, and the PC is covered by water

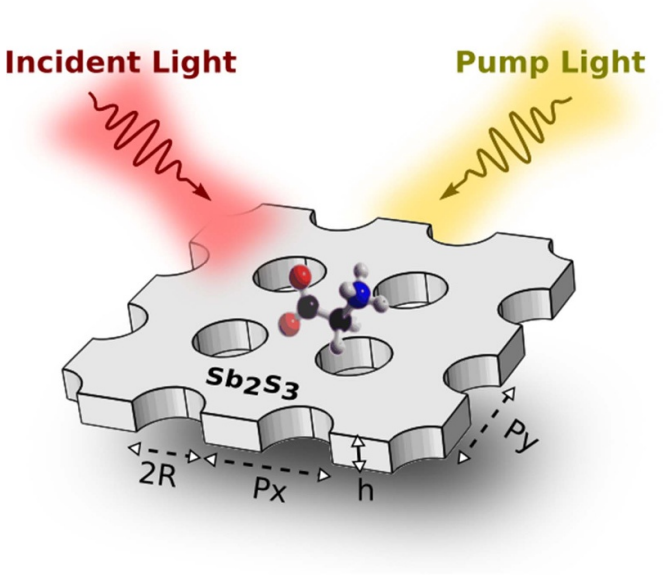

Figure 1. Perspective view of the two-dimensional photonic crystal with the periodic distribution of holes at the Sb_2S_3 substrate, excited by the y-polarized plane wave.

with 1.33 refractive index [35]. To approximate the effective permittivity of Sb_2S_3, we use a well-known theory, namely the Lorentz–Lorenz relation, as [30, 36, 37]:

$$\frac{\varepsilon_{\text{eff}}(\lambda)-1}{\varepsilon_{\text{eff}}(\lambda)+2} = L \times \frac{\varepsilon_{\text{c}}(\lambda)-1}{\varepsilon_{\text{c}}(\lambda)+2} + (L-1) \times \frac{\varepsilon_{\text{a}}(\lambda)-1}{\varepsilon_{\text{a}}(\lambda)+2}, \quad (1)$$

where $\varepsilon_{\text{eff}}(\lambda)$ is the effective permittivity of the substrate, $\varepsilon_{\text{a}}(\lambda)$ and $\varepsilon_{\text{c}}(\lambda)$ are the permittivity of amorphous and crystalline Sb_2S_3, and L is the crystallization fraction, which could vary between 0 and 1. Figure 2 illustrates the real and imaginary parts of the effective permittivity in the amorphous and crystalline phases of Sb_2S_3. As shown in this figure, the imaginary parts of this material at larger wavelengths than 700 nm are close to zero representing it as a loss-free phase change material at these wavelengths. In this section of our study, the crystallization fraction is set at $L = 0.3$ through optical pumping, which is proportional to a refractive index of 2.83. Furthermore, this crystallization fraction of phase change materials can be tuned experimentally based on [38]. As shown in this reference, adjusting optical pumping leads to controlling the transmission of the GST-Fano meta-device [38]. For the investigation, the numerical software of CST microwave studio with FDFD method is applied to the proposed structure with periodic boundary conditions (see figure 1). Also, the excitation of the numerical analysis is a y-polarized plane wave that normally radiates to the PC.

To have two sharp Fano resonances between wavelengths of 1400–1700 nm and achieve significant field improvement, the periodicities of the structure should be set at $Px = 950$ nm and $Py = 950$ nm, and the radius of the holes and the thickness of the substrate are equal to $R = 75$ nm and $t = 250$ nm,

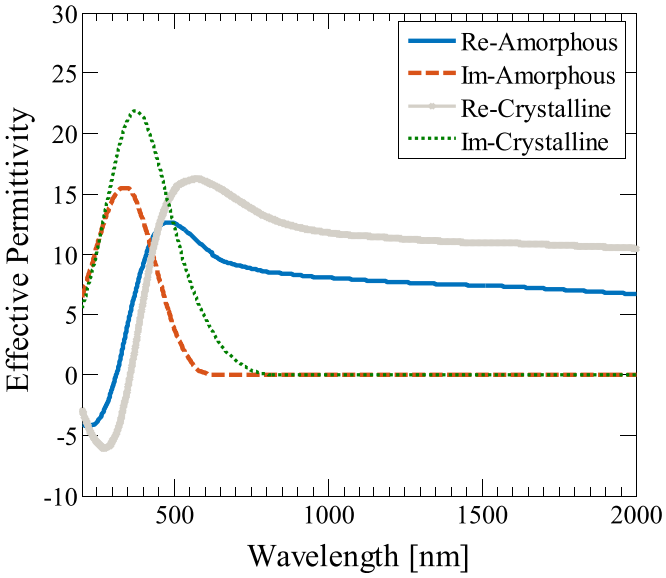

Figure 2. Real and imaginary parts of the effective permittivity in the amorphous and crystalline phase of Sb_2S_3.

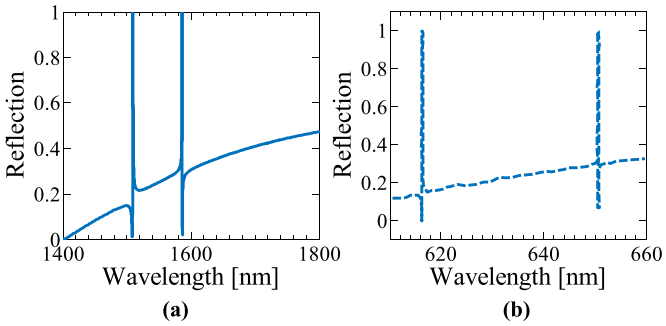

Figure 3. (a) The reflection of the two-dimensional photonic crystal, excited by a *y*-polarized plane wave with the periodicities of $Px = 950$ nm and $Py = 950$ nm at the directions of the *x*-axis and *y*-axis. (b) Reflection of the 2D PC of [8] with the structural parameters of $R = 20$ nm, and $Px = Py = 400$ nm.

respectively, determined by parametric simulations. As shown in figure 3(a), the two resonances, at wavelengths of 1586.4 nm and 1508.3 nm, increase the reflection close to unity, leading to field enhancement at the surface of the PC. In figure 3(b), we show the reflection from the structure of [8], which is a PC made of TiO_2 with structural parameters of $R = 20$ nm and $Px = Py = 400$ nm. Based on the numerical results from figure 3, increasing the periodicity and diameter of the holes while fixing the refractive index of the substrate (the refractive index of TiO_2 at the visible wavelengths is close to the refractive index of Sb_2S_3 around 1550 nm) leads to shifting the Fano resonances to larger wavelengths. The electric field profile of the proposed two resonances is illustrated in figures 4(a), (c) and (b), (d). These figures show that for the wavelength of 1586.4 nm, the electric field enhancement was improved in the water at the top part of the PC and realized as strips. Also,

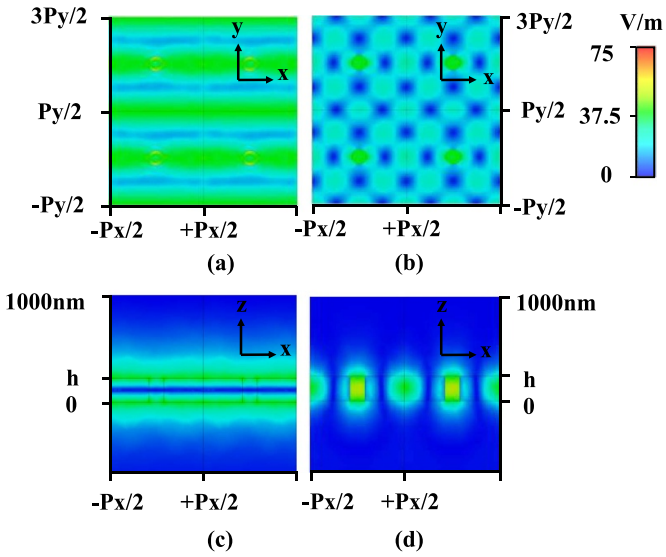

Figure 4. The electric field profiles at (a), (b) the top view and (c), (d) the side view of the photonic crystal, which are related to the (a), (c) the first resonance (Raman resonance) in the wavelength of 1586.4 nm and (b), (d) the second resonance (Rayleigh resonance) in the wavelength of 1508.3 nm.

the electric field profile for the wavelength of 1508.3 nm is enhanced, such as a raster form, inside and around the holes at the proposed substrate that have significant applications in sensing and Raman spectroscopy due to the existence of hot-spots, which is proper for molecular detection.

The radius of the holes in the proposed structure can affect the wavelength of the second resonance (Rayleigh resonance) and has a significant impact on the electric field profile at the surface and bulk of the PC. As shown in figure 5(a), the wavelength of the second resonance varies from 1497 nm for a hole radius of 95 nm to 1527 nm for a hole radius of 35 nm. However, the first resonance (Raman resonance) is almost unchanged around the wavelength of 1586 nm, representing a low dependency on the radius of holes. This behavior is predictable based on the electric field profile (see figure 4(a)), in which variation in the radius of holes has no impact on the electric field profile. Moreover, it can be inferred from figure 5(a) that as the radius of the holes increases, the bandwidth of the proposed Fano resonances increases, leading to the dropping of the quality factor and SERS enhancement of the structure. Figure 5(b) illustrates the variation of the SERS enhancement versus the radius of the holes for Rayleigh resonance. As shown in this figure, this enhancement at the surface of the PC is equal to 208, achievable for a hole radius of 45 nm, and it could be a suitable selection for the optimum structure. The electric field profile of the first resonance is the other significant parameter that depends on the radius of the holes in the PC. As can be seen in figures 5(c)–(f), the increasing radius of the holes in the PC causes a diminishing size of nulls in the field profile, which is proper for the detection of the biomolecule.

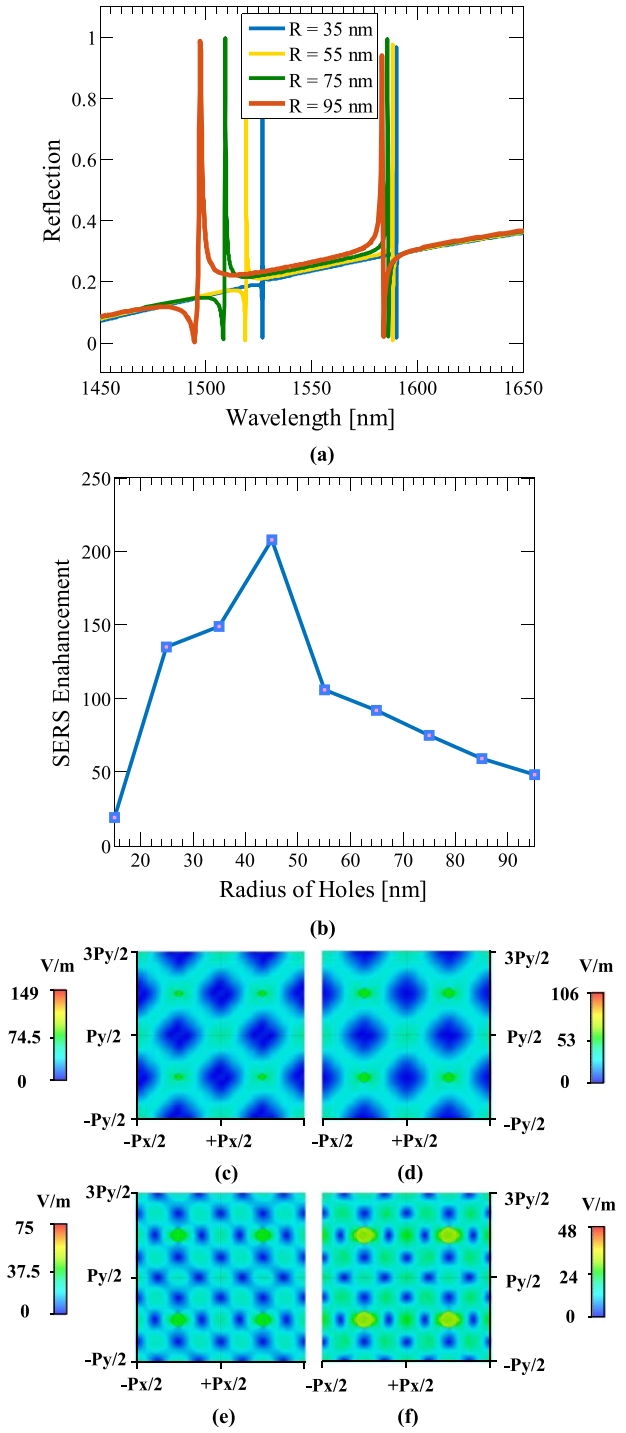

Figure 5. (a) The reflection of the two-dimensional photonic crystal in the wavelength range of the incident light for the different radii of the holes and (b) the SERS enhancement versus the variation of hole radius between (15–95 nm) for the second resonance. The electric field profile of the second resonance when the radius of the holes is set at (c) 35 nm, (d) 55 nm, (e) 75 nm, and (f) 95 nm.

3. Tune and compensate the error Raman resonance wavelength

The novel feature of this work is tuning the proposed Fano resonances by optical pumping. As represented in the previous section, the tuning of Fano resonances occurs by variation in the diameter of holes and periodicity of the PC in the direction of the *x*-axis and *y*-axis. According to this point that the refractive index tuning is equal to changing the physical parameter of the structure, the real-time tuning without changing the dimensions of the structure can be achieved by adjusting the permittivity of Sb_2S_3. Thus, changing the effective permittivity of Sb_2S_3 in a small range between 7.16–10.76 due to variations in optical pumping leads to tuning resonances in a specific range of wavelengths. To investigate this feature, we set the radius of holes at 45 nm to realize the optimum structure, and the crystallization fraction varies from $L = 0$ for an effective permittivity of 7.16 in the amorphous phase to $L = 1$ for an effective permittivity of 10.76 in the crystalline phase of Sb_2S_3. As shown in figure 6, this variation in permittivity causes a change in the wavelength of the first Fano resonance between 1551 nm and 1689 nm. In contrast, the wavelength of the second Fano resonance changes from 1451 nm to 1683 nm. This degree of freedom, especially for the first resonance (Raman resonance), which is equal to 138 nm, provides the possibility of detecting different biomolecules at different wavelengths of light. Moreover, tuning optical pumping can control the distance between the first and second resonances and realize a strong matched Fano resonance with a high SERS enhancement.

Tuning the Raman resonance is one of the most significant results of this work. However, the realization of this structure through available technology may not be possible. The critical problem is the fabrication of the PC with the exact location and radius of holes with an accuracy of less than 5 nm. Failure to achieve this accuracy will result in shifting of the calculated resonances, which have not been considered in previous works [8–12, 16–19, 24–30], leading to wasted effort in designing and analyzing structures for SERS enhancement. As a result, to compensate for this significant issue, we have adjusted the refractive index of the Sb_2S_3 substrate utilizing optical pumping. For instance, we investigated a part of the proposed PC with four holes and periodic boundary conditions (see figure 7(a)), in which the periodicity may be altered by 5 nm. Also, the radius of holes and substrate thickness is a random function with means of 45 nm and 250 nm, respectively, and a deviation of 5 nm (table 1). These errors may occur in the fabrication process, leading to a shift in the Raman resonance to 1544 nm (see figure 7(c)). So to correct this problem, the crystallization fraction should be changed from $L = 0.3$ to $L = 0.337$ until the proposed Raman resonance is located at the wavelength of 1550 nm. In another situation (investigation 2 of table 1), again the radius of holes, the thickness of the substrate, and periodicities are random functions similar to investigation 1, causing the Raman resonance to be placed at 1565 nm (see figure 7(d)). Consequently, the proposed resonance is set at 1550 nm by changing the optical pumping through crystallization fraction from $L = 0.3$ to $L = 0.19$. In the last situation (investigation 3 of table 1), occurring errors in the radius of holes, the thickness of the substrate, and periodicities lead to the proposed resonance being placed at the wavelength of 1554 nm (see figure 7(e)). As a solution to this problem, the crystallization

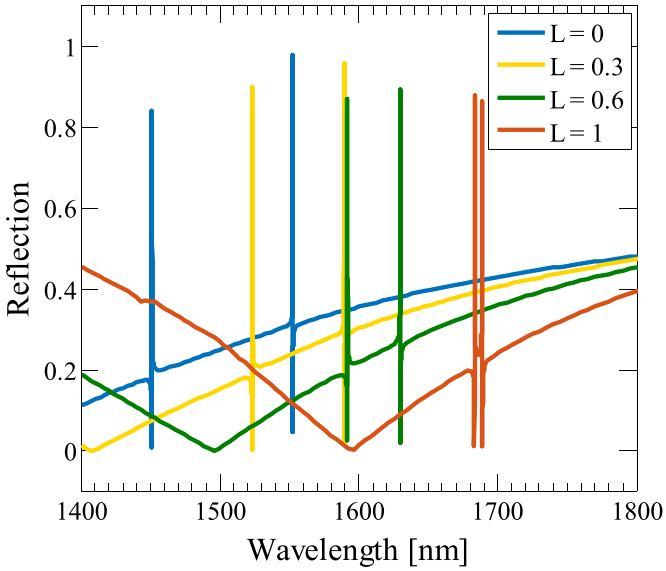

Figure 6. The reflection of the two-dimensional photonic crystal at different wavelengths of the incident light for the variation of optical pumping when the periodicities are $Px = 950$ nm and $Py = 950$, respectively, and the radius of holes is equal to 45 nm.

fraction was tuned at $L = 0.265$ until the resonance was set at 1550 nm.

The keynote is the dependency of the proposed two resonances on the periodicity of the structure in the x-axis and y-axis directions. Based on figure 8(a), variation in the periodicity from 900 nm to 1050 nm causes the wavelength of the second resonance to change from 1488 nm to 1575 nm while keeping the first resonance at 1586.4 nm. Furthermore, changing the periodicity in the direction of the y-axis leads to changing both the first and second resonances, as shown in figure 8(b). As shown in this figure, the first and second resonances vary in the wavelength range of (1537–1617 nm) and (1490–1540 nm), respectively. Using this critical feature of the proposed PC, we can adjust the first and second resonances to match each other at the same wavelength, leading to uniformity of the electric field at the surface of the PC. This uniformity is significant, especially when the attached molecules are not placed at the hot spot of the electric field profile (see figure 4) on the PC surface.

4. Realization of uniform matched Fano resonance

In this section, we match the first and second resonances with each other to achieve uniform electric field enhancement at the surface of the PC. To realize such a significant purpose, both periodicities in the x-axis and y-axis directions are tuned to reach the matched Fano resonance at a wavelength of 1550 nm. Using parametric simulations, the periodicities are set at $Px = 1051.91$ nm and $Py = 909.35$ nm, resulting in the excitation of both the first and second resonances simultaneously, as shown in figure 9(a). This diagram illustrates how both resonances overlap and contribute to uniform and significant field enhancement in figures 9(b) and (c), reaching a maximum improvement of 1200. This uniformity causes that placing biomolecules in different parts of the PC will not have a significant effect on the detection and sensitivity of Raman spectroscopy.

To have a tangible benchmark for uniformity, we use equation (2) as [8]:

$$UF = \frac{\frac{1}{(P_x P_y)^2}\left|\int_0^{P_y}\int_0^{P_x} E(x,y)\mathrm{d}x\mathrm{d}y\right|^2}{\frac{1}{(P_x P_y)}\int_0^{P_y}\int_0^{P_x} |E(x,y)|^2\mathrm{d}x\mathrm{d}y} \tag{2}$$

where Px and Py are the periodicities of the PC in the direction of the x-axis and y-axis, respectively, and E(x, y) is the electric field between the PC and water. According to equation (2), the uniformity of the PC at the matched Fano resonance at 1550 nm is 93%, which indicates that both resonances were successfully matched. The average and maximum SERS enhancements of this resonance are 512 and 1052, respectively, calculated based on the electric field profile of figure 9(b), and the SERS enhancement factor can be determined according to equation (3) as [39]:

$$EF = \left(\frac{|E|}{|E_0|}\right)^2_{\lambda_{\text{Rayleigh}}} \times \left(\frac{|E|}{|E_0|}\right)^2_{\lambda_{\text{Raman}}} \tag{3}$$

where the magnitude of the electric field in the first and second terms is related to Rayleigh and Raman wavelengths. The proposed SERS enhancement factor in this work is calculated as 1.23×10^{12}, which is more than previous works [8, 17, 34, 40–45]. Also, the quality factor of this matched resonance reaches

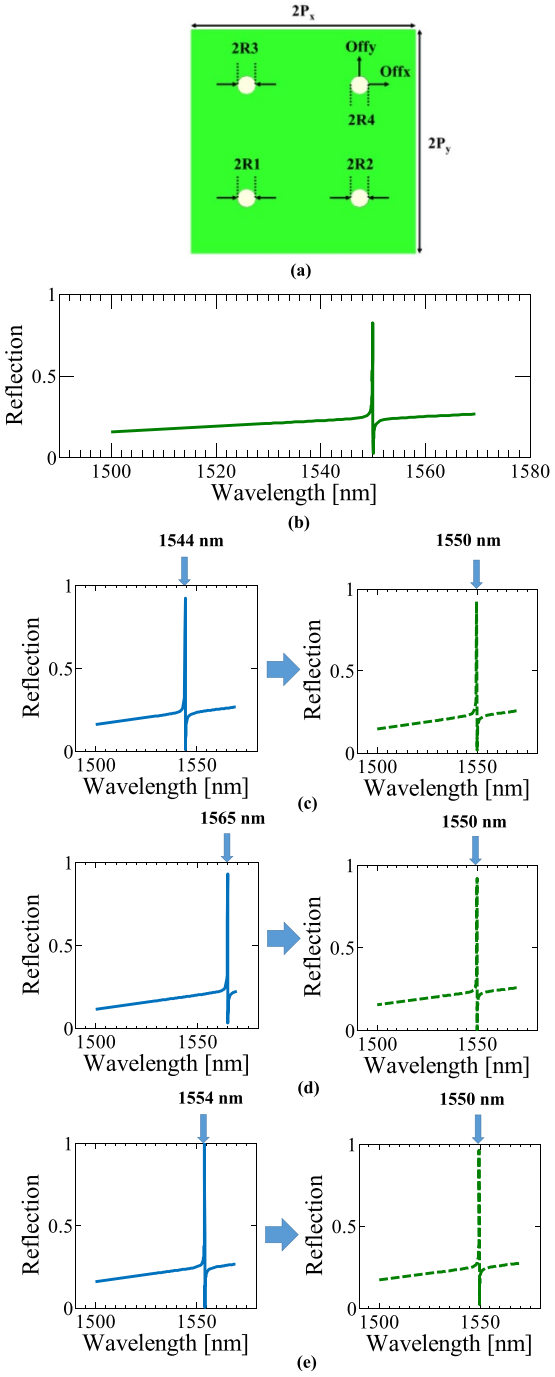

Figure 7. (a) Schematic of the basic photonic crystal and (b) the Raman resonance, tuned at the wavelength of 1550 nm with periodicities of $Px = 909.4$ nm and $Py = 909.4$ nm. (c) Error in the proposed resonance when the photonic crystal has the parameters in table 1 (investigation 1), and compensating error with the crystallization fraction of $L = 0.337$. (d) Another error occurs in the Raman resonance when the photonic crystal has the parameters in table 1 (investigation 2), and compensating it using the crystallization fraction of $L = 0.19$. (e) Occurring errors in the Raman resonance in the third investigation 3, and compensating it by setting the crystallization fraction at $L = 0.265$.

$Q = 24\,618.3$ based on the criteria of center frequency divided by the frequency offset from the center frequency where the response falls by 3 dB.

Table 2 shows the characteristics of the proposed structure and other previous works for the SERS enhancement application. As can be seen in this table, using the PC, we achieved one of the highest SERS enhancements with a uniformity of 93%, while most previous works did not investigate this significant parameter. Also, the possibility of a reconfigurable structure has been realized in our work, which is one of the most prominent advantages of the present research. Moreover, based on table 2, the proposed structure in this

Table 1. Different photonic crystal investigations with several parameter errors that may have occurred in the fabrication process.

Par[a]	Basic (nm)	Inv[b] 1 (nm)	Inv 2 (nm)	Inv 3 (nm)
Hole 1	45	50	45	50
Hole 2	45	45	50	40
Hole 3	45	40	50	50
Hole 4	45	40	45	45
Off*x*	0	+5	−5	−5
Off*y*	0	0	−5	0
Thick of Sub[c]	250	250	255	250
Px	909.4	904.4	914.4	909.4
Py	909.4	904.4	914.4	914.4
λ[d]	1550	1544	1565	1554

[a] Parameter.
[b] Investigation.
[c] Thickness of substrate.
[d] Wavelength of the resonance.

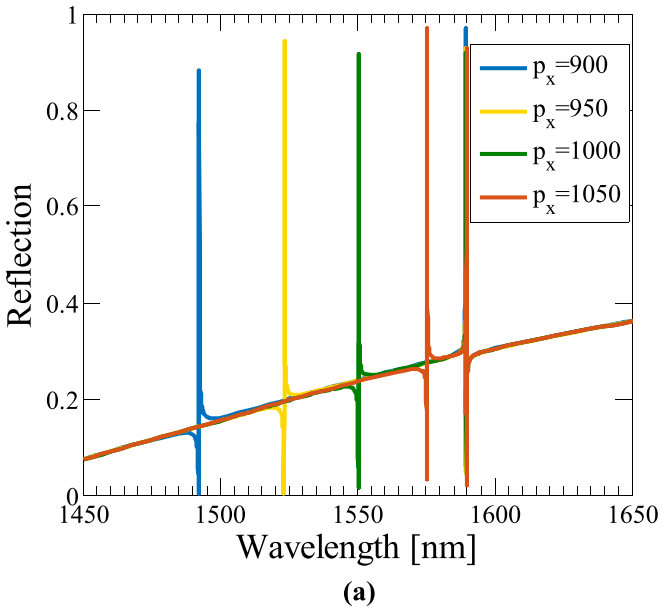

Figure 8. The reflection of the two-dimensional photonic crystal at different wavelengths of the incident light when (a) *Py* is equal to 950 nm and *Px* is varied in the range of 900–1050 nm. (b) *Px* is equal to 950 nm, and the variation of *Py* is in the range of 900–975 nm.

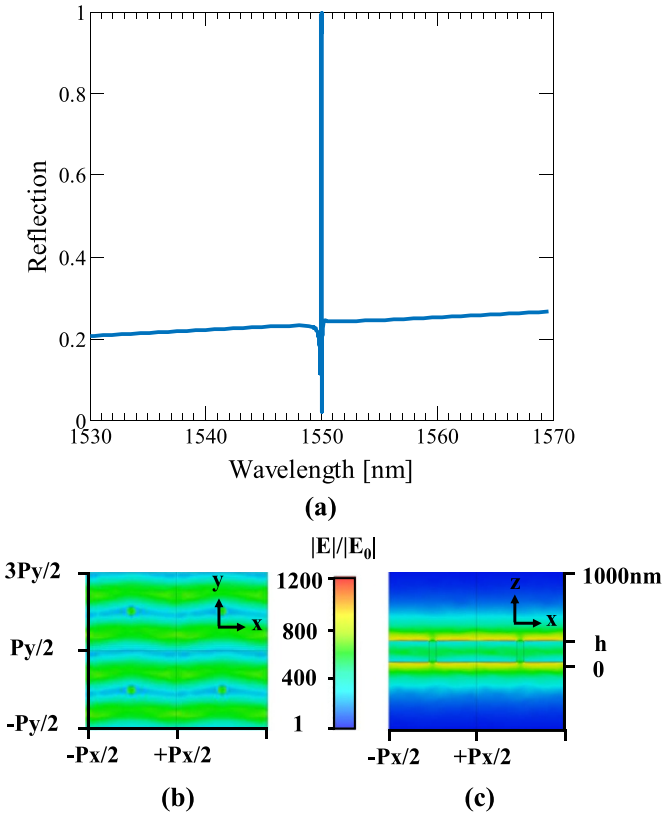

Figure 9. (a) Matched Fano resonance of the photonic crystal at the wavelength of 1550 nm is realized by tuning periodicities at Px = 1051.91 nm and Py = 909.35 nm. (b), (c) The electric field profile of the photonic crystal in the proposed Fano resonance, which is reached to the maximum field enhancement of 1052.

Table 2. Comparing the characteristics of previous works for the application of SERS enhancement and the presented work in this paper.

References	SERS enhnc factor[a]	Uniformity	Type of structure	St/Rc[b]
[42]	3.01×10^5	No	NP[c] with multi-layer	St
[41]	5.26×10^5	No	NP	St
[39]	1.2×10^7	Almost	NP	St
[8]	2.4×10^7	97%	A flat layer	St
[43]	4.6×10^7	No	Textured platform	St
[40]	6.77×10^7	No	NP	St
[45]	10^8	No	Core–shell NP	St
[10]	6.4×10^9	No	Grating	St
[34]	4.1×10^{10}	No	NP	St
[44]	1.4×10^{11}	No	NP	St
This Work	1.23×10^{12}	93%	A flat layer	Rc

[a] SERS enhancement factor.
[b] Static/reconfigurable.
[c] Nano-particles.

study does not have a complicated fabrication procedure. This structure can be fabricated using e-beam lithography, one of the most accurate methods of nano-device fabrication, in which the Sb_2S_3 substrate is deposited by spin coating. After using the resist layer and mask on the substrate, the focused e-beam forms an image in the resist, and finally, the etching process can be applied to create holes in the substrate.

5. Conclusion

In this paper, we proposed a novel architecture for the application of SERS enhancement. A Sb_2S_3 all-dielectric PC was employed to reduce scattering due to its ability to support high-quality Fano resonances. The proposed PC was studied using numerical analysis with the FDFD method. In this work, tuning optical pumping could change the wavelength of

the Raman and Rayleigh resonances in the range of (1551–1689 nm) and (1451–1683 nm), respectively. This tuning of resonance wavelengths, which is realized by changing optical pumping, gives us the ability to sense different molecules of different sizes in the future. Moreover, compensation for the error in different parameters of the structure, such as the location and radius of holes, periodicities, and thickness of the PC, occurring through the fabrication process, was realized by controlling the crystallization fraction. In this analysis, the adjustment to the structure provided matched Fano resonance led to a uniform and high SERS enhancement factor of 1.23×10^{12}, which is significant for imaging applications and Raman spectroscopy.

Data availability statement

The data cannot be made publicly available upon publication because no suitable repository exists for hosting data in this field of study. The data that support the findings of this study are available upon reasonable request from the authors.

ORCID iDs

Mohammad Ali Shameli https://orcid.org/0000-0002-4795-7470
Mohammad Reza Eskandari https://orcid.org/0000-0002-3819-378X

References

[1] Lai H, Li G, Xu F and Zhang Z 2020 Metal–organic frameworks: opportunities and challenges for surface-enhanced Raman scattering–a review *J. Mater. Chem.* C **8** 2952–63
[2] Cheng Q, Miao Y, Zhang R, Min W and Yang Y 2022 Applications of stimulated Raman scattering (SRS) microscopy in materials science *Stimulated Raman Scattering Microscopy* (Amsterdam: Elsevier) pp 515–27
[3] Vlasov A V *et al* 2020 Raman scattering: from structural biology to medical applications *Crystals* **10** 38
[4] Bharati M S S and Soma V R 2021 Flexible SERS substrates for hazardous materials detection: recent advances *Opto-Electron. Adv.* **4** 210048–1
[5] Lin S, Cheng Z, Li Q, Wang R and Yu F 2021 Toward sensitive and reliable surface-enhanced Raman scattering imaging: from rational design to biomedical applications *ACS Sens.* **6** 3912–32
[6] Cheng Z, Premasiri R, Lin H, Huang Y, Zhang C, Yang C, Ren B, Ziegler L D and Cheng J X 2019 Plasmon-enhanced stimulated Raman scattering microscopy with single-molecule detection sensitivity *Nat. Commun.* **10** 1–11
[7] Lee H K, Lee Y H, Koh C S L, Phan-Quang G C, Han X, Lay C L, Sim H Y F, Kao Y C, An Q and Ling X Y 2019 Designing surface-enhanced Raman scattering (SERS) platforms beyond hotspot engineering: emerging opportunities in analyte manipulations and hybrid materials *Chem. Soc. Rev.* **48** 731–56
[8] Sabri L, Shahabadi M, Forooraghi K and Ghaffari-Miab M 2020 Interaction of two guided-mode resonances in an all-dielectric photonic crystal for uniform SERS *Opt. Express* **28** 10467–76
[9] Kalachyova Y, Mares D, Lyutakov O, Kostejn M, Lapcak L and Svorcik V 2015 Surface plasmon polaritons on silver gratings for optimal SERS response *J. Phys. Chem. C* **119** 9506–12
[10] Iqbal T, Ashfaq Z, Afsheen S, Ijaz M, Khan M Y, Rafique M and Nabi G 2020 Surface-enhanced Raman scattering (SERS) on 1D nano-gratings *Plasmonics* **15** 1053–9
[11] Tang Z, Wu J, Yu X, Hong R, Zu X, Lin X, Luo H, Lin W and Yi G 2021 Fabrication of Au nanoparticle arrays on flexible substrate for tunable localized surface plasmon resonance *ACS Appl. Mater. Interfaces* **13** 9281–8
[12] Wu S, Shen Y and Jin C 2019 Surface-enhanced Raman scattering induced by the coupling of the guided mode with localized surface plasmon resonances *Nanoscale* **11** 14164–73
[13] Zhang C, Li Z, Qiu S, Lu W, Shao M, Ji C, Wang G, Zhao X, Yu J and Li Z 2022 Highly ordered arrays of hat-shaped hierarchical nanostructures with different curvatures for sensitive SERS and plasmon-driven catalysis *Nanophotonics* **11** 33–44
[14] Zhang C, Ji C, Yu J, Li Z, Li C, Xu S, Li W, Man B and Zhao X 2021 MoS_2-based multiple surface plasmonic coupling for enhanced surface-enhanced Raman scattering and photoelectrocatalytic performance utilizing the size effect *Opt. Express* **29** 38768–80
[15] Ji C, Lu J, Shan B, Li F, Zhao X, Yu J, Xu S, Man B, Zhang C and Li Z 2022 The origin of Mo_2C films for surface-enhanced Raman scattering analysis: electromagnetic or chemical enhancement? *J. Phys. Chem. Lett.* **13** 8864–71
[16] Pokhriyal A, Lu M, Chaudhery V, George S and Cunningham B T 2013 Enhanced fluorescence emission using a photonic crystal coupled to an optical cavity *Appl. Phys. Lett.* **102** 221114
[17] Pirotta S *et al* 2013 Surface-enhanced Raman scattering in purely dielectric structures via Bloch surface waves *J. Phys. Chem. C* **117** 6821–5
[18] Lagarkov A, Boginskaya I, Bykov I, Budashov I, Ivanov A, Kurochkin I, Ryzhikov I, Sedova M, Zverev A and Sarychev A K 2017 Light localization and SERS in tip-shaped silicon metasurface *Opt. Express* **25** 17021–38
[19] Romano S, Zito G, Penzo E, Yépez S N L, Cabrini S, De Luca A C, Rendina I and Mocella V 2019 Enhancing light-matter interaction in all-dielectric photonic crystal metasurfaces *Proc. SPIE* **11028** 110280I
[20] Kassa-Baghdouche L and Cassan E 2018 Mid-infrared refractive index sensing using optimized slotted photonic crystal waveguides *Photon. Nanostruct: Fundam. Appl.* **28** 32–36
[21] Kassa-Baghdouche L 2019 Cassan E, Sensitivity analysis of ring-shaped slotted photonic crystal waveguides for mid-infrared refractive index sensing *Opt. Quantum Electron.* **51** 1–11
[22] Kassa-Baghdouche L 2019 Optical properties of a point-defect nanocavity-based elliptical-hole photonic crystal for mid-infrared liquid sensing *Phys. Scr.* **95** 015502
[23] Kassa-Baghdouche L, Boumaza T and Bouchemat M 2015 Optimization of Q-factor in nonlinear planar photonic crystal nanocavity incorporating hybrid silicon/polymer material *Phys. Scr.* **90** 065504
[24] Eskandari M R, Shameli M A and Safian R 2022 Analysis of an electrically reconfigurable metasurface for manipulating polarization of near-infrared light *J. Opt. Soc. Am.* B **39** 145–54
[25] Liu Y, Mao R, Zhang P, Li W, Wang M, Zhang L, Gong Y, Zhou P, Liang D and Deng L 2022 Numerical study of mid-infrared tunable metalenses based on $Ge_2Sb_2Te_5$ phase-change material *J. Appl. Phys.* **55** 244003

[26] Shameli M A, Eskandari M R and Safian R 2022 Unidirectional radiation control of quantum emitters coupled to spiral nano-antennas using optoelectronic material in near-infrared *Opt. Commun.* **517** 128345
[27] Shameli M A, Eskandari M R and Safian R 2022 Rotational freedom thin-film solar cell using a reconfigurable nano-antenna with 4-dimethyl-amino-N-methyl-4-stilbazolium tosylate *IET Optoelectron.* **16** 179–87
[28] Tripathi A *et al* 2021 Tunable Mie-resonant dielectric metasurfaces based on VO_2 phase-transition materials *ACS Photonics* **8** 1206–13
[29] Huang Y, Wang Y, Zhang L, Shao Y, Zhang F, Liao C and Wang Y 2019 Tunable electro-optical modulator based on a photonic crystal fiber selectively filled with liquid crystal *J. Lightwave Technol.* **37** 1903–8
[30] Delaney M, Zeimpekis I, Lawson D, Hewak D W and Muskens O L 2020 A new family of ultralow loss reversible phase-change materials for photonic integrated circuits: Sb_2S_3 and Sb_2Se_3 *Adv. Funct. Mater.* **30** 2002447
[31] Limonov M F, Rybin M V, Poddubny A N and Kivshar Y S 2017 Fano resonances in photonics *Nat. Photon.* **11** 543–54
[32] Lane L A, Xue R and Nie S 2018 Emergence of two near-infrared windows for *in vivo* and intraoperative SERS *Curr. Opin. Chem. Biol.* **45** 95–103
[33] Song J, Zaccaria R P, Yu M B and Sun X W 2006 Tunable Fano resonance in photonic crystal slabs *Opt. Express* **14** 8812–26
[34] Fang Y, Seong N H and Dlott D D 2008 Measurement of the distribution of site enhancements in surface-enhanced Raman scattering *Science* **321** 388–92
[35] Hale G M and Querry M R 1973 Optical constants of water in the 200-nm to 200-μm wavelength region *Appl. Opt.* **12** 555–63
[36] Abdollahramezani S, Taghinejad H, Fan T, Kiarashinejad Y, Eftekhar A A and Adibi A 2018 Reconfigurable multifunctional metasurfaces employing hybrid phase-change plasmonic architecture (arXiv:1809.08907)
[37] Chu C H *et al* 2016 Active dielectric metasurface based on phase-change medium *Laser Photon. Rev.* **10** 986–94
[38] Pitchappa P, Kumar A, Prakash S, Jani H, Venkatesan T and Singh R 2019 Chalcogenide phase change material for active terahertz photonics *Adv. Mater.* **31** 1808157
[39] He S, Chua J, Tan E K M and Kah J C Y 2017 Optimizing the SERS enhancement of a facile gold nanostar immobilized paper-based SERS substrate *RSC Adv.* **7** 16264–72
[40] Lee S Y, Hung L, Lang G S, Cornett J E, Mayergoyz I D and Rabin O 2010 Dispersion in the SERS enhancement with silver nanocube dimers *ACS Nano* **4** 5763–72
[41] Litti L and Meneghetti M 2019 Predictions on the SERS enhancement factor of gold nanosphere aggregate samples *Phys. Chem. Chem. Phys.* **21** 15515–22
[42] Zhou C, Sun L, Zhang F, Gu C, Zeng S, Jiang T, Shen X, Ang D S and Zhou J 2019 Electrical tuning of the SERS enhancement by precise defect density control *ACS Appl. Mater. Interfaces* **11** 34091–9
[43] Kowalska A A, Kaminska A, Adamkiewicz W, Witkowska E and Tkacz M 2015 Novel highly sensitive Cu-based SERS platforms for biosensing applications *J. Raman Spectrosc.* **46** 428–33
[44] Cañamares M V, Garcia-Ramos J V, Sanchez-Cortes S, Castillejo M and Oujja M 2008 Comparative SERS effectiveness of silver nanoparticles prepared by different methods: a study of the enhancement factor and the interfacial properties *J. Colloid Interface Sci.* **326** 103–9
[45] Qian X M and Nie S M 2008 Single-molecule and single-nanoparticle SERS: from fundamental mechanisms to biomedical applications *Chem. Soc. Rev.* **37** 912–20